TREND

Trapped Radiation Environment Model Development

Time Dependent Radiation-Belt Space Weather Modelling

ESA/TOS-EMA Contract No. 11711/95/NL/JG - CCN 1 to Work Order No. 3

Technical Note 2A

Review of the source and loss processes for low-altitude trapped protons

M. Kruglanski

(July 1998)

B.I.R.A. – I.A.S.B.	D.E.R.T.S.	P.S.I.
Avenue Circulaire 3 B-1180 Brussel Belgium	ONERA CERT BP 4025 F-31055 Toulouse cedex 4 France	Laboratory for Astrophysics CH-5232 Villigen Switzerland

ESA Technical Management: E.J. Daly (WMA)

Chapter 1

Notations and definitions

The radiation belt proton population can be fully described by a six-dimensional density function $F(\mathbf{p}, \mathbf{q}, t)$ in the phase space where **p** and **q** are the particle momentum and the position coordinate, respectively. The number d^6N of protons in the volume d^3pd^3q is then given by

$$d^6N = F(\mathbf{p}, \mathbf{q}, t)d^3\mathbf{p}d^3\mathbf{q} \tag{1.1}$$

For radiation belt calculations, a phase spaces which is related to adiabatic invariants and their conjugate phase coordinates φ_i, are used instead of the position-momentum space. The adiabatic invariants J_i are defined by the path integrals

$$J_i = \oint[\mathbf{p} + q\mathbf{A}] \cdot d\mathbf{l} \tag{1.2}$$

where **A** is the electromagnetic vector potential and q is the particle charge. The closed integral is evaluated for the three distinct forms of quasi-periodic motion of the trapped particles: gyration about the magnetic field line, oscillation between magnetic mirror points and azimuthal drift around the Earth. The three invariants J_1, J_2 and J_3 are associated with the gyration, bounce and drift motions of the particle, respectively. Due to the time scale of these motions, the particle phases φ_i can not be distinguished generally by observation and only a phase averaged density function $f(J_i, t)$ is considered.

The first adiabatic invariant is given by

$$M \equiv \frac{q}{2m_0}J_1 = \frac{p_\perp^2}{2m_0B} \tag{1.3}$$

where m_0 is the rest mass of the particle, $p_\perp$ is the component of **p** normal to the magnetic field and *B* is the intensity of the magnetic field. The second adiabatic invariant is defined by

$$J \equiv J_2 = \oint p_{||}ds \tag{1.4}$$

where $p_{\|}$ is the component of **p** parallel to **B** and is integrated along the bounce path. When the particle momentum is constant during one bounce (no parallel forces and time variations slow compared with a bounce period), the integral invariant coordinate

$$I = \frac{J}{2p} \tag{1.5}$$

is often used. The integral invariant depends only on the magnetic field geometry and is given by

$$I = \int_{s_m}^{s'_m} \sqrt{1 - B(s)/B_m}\, ds \tag{1.6}$$

where s_m and s'_m are the locations of the mirror points along the field line segment and B_m is the magnetic field intensity at these mirror points. The third adiabatic invariant is given by the magnetic flux enclosed by the drift shell:

$$\Phi = \iint \mathbf{B} \cdot d\mathbf{S} \tag{1.7}$$

where $d\mathbf{S}$ is an element of a surface enclosed by the drift path.

The time evolution of the phase averaged density function $f(J_i, t)$ by a linear Fokker-Planck equation of the form

$$\frac{\partial f}{\partial t} = -\sum_i \frac{\partial}{\partial J_i}[C_i f] + \sum_i \frac{\partial}{\partial J_i} \sum_j \left[D_{ij} \frac{\partial}{\partial J_j} \right] + S - Q \tag{1.8}$$

where C_i are the friction terms, D_{ij} the diffusion coefficients, S the sources and Q the losses. In order to get more convenient variables, coordinate transformations are usually applied to the Fokker-Planck equation. The introduced variables are, for instance, the kinetic energy E, L parameters, the equatorial pitch-angle α_0, and the derived invariant K.

The L parameter is originally defined in a pure magnetic dipole field to label the field line. It corresponds to the distance from the dipole centre to the equatorial crossing (or minimum B value) of a field line, and is expressed in Earth's radii. This definition has been extended in different way for more realistic configurations of the Earth's magnetic field. The most common definition links the parameter L as a function of the pair (I, B_m) by

$$\frac{L_m^3 R_E^3 B_m}{M_0} = H\left(\frac{I^3 B_m}{M_0} \right) \tag{1.9}$$

where M_0 is an arbitrary dipole magnetic moment (e.g. $0.311653\ G\,R_E^3$) and H a function tabulated by McIlwain. Another definition, introduced by Roederer, links the parameter L with the third adiabatic invariant by

$$L^* = \frac{2\pi M_0}{\Phi R_E} \tag{1.10}$$

which as the advantage to be also an invariant but which is more expensive to compute than L_m. In the only case of a pure dipolar magnetic field with momentum equal to M_0, both definitions are equivalent.

The equatorial pitch-angle α_0 is defined as the angle between **p** and **B** at the point of minimum B value of the field line along which the particle is bouncing. By conservation of the first adiabatic invariant,

$$\sin\alpha_0 = \sqrt{B_0/B_m} \tag{1.11}$$

where B_0 is the minimum B value. It is generally convenient to let $B_0 \equiv M_0/L_m^3$ such that.

$$\sin\alpha_0 = \frac{1}{\sqrt{H(I^3 B_m/M_0)}} \tag{1.12}$$

The second adiabatic invariants can then be rewritten as

$$J = \frac{2L_m R_E}{c} Y(\sin\alpha_0)\sqrt{E(E+2m_0c^2)} \tag{1.13}$$

where Y is a special function linked to the function H by the relation

$$H[xY^3(x^{-1/2})] = x \tag{1.14}$$

The derived invariant is defined by

$$K \equiv \frac{J}{\sqrt{8m_0 M}} = I\sqrt{B_m} \tag{0.1}$$

which is conserved in absence of parallel external forces.

References

[1.1] Roederer, J.G., 1970: Dynamics of Geomagnetically Trapped Radiation, Springer-Verlag

[1.2] Schulz, M., 1991: The Magnetosphere, in Geomagnetism, vol. 4, ed. P. Jacobs, Academic Press, 87-293

[1.3] Walt, M., 1994: Introduction to Geomagnetically Trapped Radiation, in Cambridge atmospheric and space science series, ed. A.J. Dessler, J.T. Houghton and M.J. Rycroft, Cambridge University Press

Chapter 2

Literature review

In the first section of this chapter, the existing trapped proton models which include a time variation of the proton population are reviewed. The main physical processes are described in the second section.

2.1 Trapped proton dynamical models

2.1.1 Blanchard and Hess (1964)

Blanchard and Hess [2.8] studied the change on the proton population due to the solar cycle variation. Their study is limited to 25-600 MeV protons with L_m comprised between 1.25 and 1.6, and with the minimum altitude of their mirror points located between 300 and 600 km. The time evolution of the proton fluxes is affected by

- a CRAND source depending only on the energy and modulated in time;
- a loss term due to inelastic nuclear collisions in the atmosphere with O_2, O, Ne and He;
- a friction term due to the slowing down of protons by Coulomb scattering with atmospheric constituents (converted into equivalent oxygen atoms).

The friction term is supposed to only affect the particle energy and to leave B_m and L_m invariant. The loss and friction terms are evaluated with the help of the atmospheric model of Harris and Priester [2.16][2.17] averaged in local time, longitude and over the particle bounce path. The longitude average takes into account the altitude variation of the particle mirror points with longitude but does not take into account the variation of the drift velocity of the particles with longitude. The average on the particle bounce path is done afterwards, assuming a simple dipole field. The modulation in time of the source term is similar to the solar cycle variation of the atmospheric model. The period from 1953 to 1964 is taken to represent a typical 11-year solar cycle.

The proton fluxes for several (B_m, L_m) pairs are determined numerically as a function of the energy. The calculation is initiated with an empty population. The time evolution is then computed over successive solar cycles until the time variation of the proton population becomes almost periodic. The results show that:

- the proton fluxes never reach the steady state solutions calculated for solar minimum or maximum conditions;

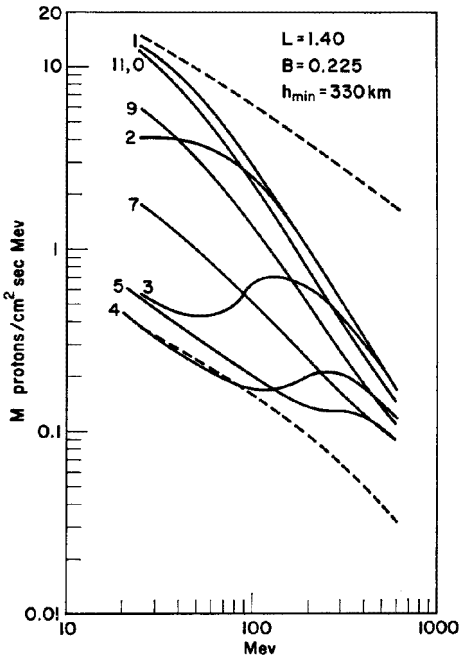

Fig. 2.1 Proton energy spectra for different epochs during the solar cycle for L_m = 1.40 and B_m = 0.225 . The curves are labelled in years from solar minimum. From [2.8].

- for the (B_m, L_m) nearest the lost cone, a peak above 100 MeV appears in the energy spectrum during the transition from solar minimum to solar maximum;
- at the lower energies, the model predicts a proton flux variation of a factor 10 or greater.

A typical result of the study is given in Fig. 2.1 where the proton energy spectrum at L_m = 1.40 , B_m = 0.225 is displayed for different epochs during the solar cycle. The upper and lower dashed lines represent the steady states for solar minimum and maximum, respectively. The solid lines are labelled with the time in years from solar minimum. During the whole solar cycle, the flux varies by a factor 3 at 400 MeV, a factor 20 at 100 MeV and a factor 35 at 50 MeV. The spectral peak clearly appears on curves 3 and 4. It is due to the fact that protons of different energies does not react with the same time-lag to the atmospheric changes.

2.1.2 Dragt (1971)

Dragt [2.12] studied the time variation of proton flux due to the solar cycle modulation of the atmosphere. His study is restricted to the high energy protons mirroring deeply in the atmosphere such that the proton lifetimes are much smaller than the time scales of transport and acceleration mechanisms. The restriction allows the diffusion processes to be neglected. The resulting model is designed for 10-800 MeV protons with L_m between 1.25 and 2.5, and is described by a transport equation which includes:

- a time independent CRAND source function of L_m and α_0 ;
- a loss term due to inelastic nuclear collisions in the atmospheric constituents;
- a friction term due to the slowing down of protons by Coulomb scattering with atmospheric constituents.

The friction term is supposed to only affect the particle energy and to leave B_m and L_m invariant. The dependence in (α_0, L_m) of the CRAND source is obtained from a dipolar approximation [2.13]. The energy dependence of the source, loss and friction terms are assumed to follow exact power laws such that, by a series of substitutions, the solution of the transport equation

can be reduced to the numerical evaluation of two simple definite integrals. For the loss and friction terms, the densities of the atmospheric constituents are supposed to be purely proportional to the atmospheric density of atomic electrons. The mean electronic atmospheric density is based on the results of Cornwall et al. [2.11] obtained for different drift shells and for different atmospheric conditions with the Harris and Priester atmosphere [2.16][2.17] and several geomagnetic field models (e.g. [2.19]). The Cornwall et al. [2.11] results have been fitted by Dragt [2.12] to the function

$$\bar{\rho}_e = a\exp[b(S-100)] \tag{2.1}$$

where the parameters *a* and *b* are function of B_m and L_m, and *S* is the time-dependant parameter of Harris and Priester.

The Dragt's model evaluates the time evolution of the proton flux spectrum for fixed values of *a* and *b*, i.e. of B_m and L_m. From several simulations computed for the whole period of time from 1956 to 1967, it results that

- the low energy proton fluxes, due to the short lifetime of the proton, almost inversely follow the atmospheric time variation;
- the high energy proton fluxes, because of longer lifetimes, show less variation;
- the proton flux falls when $\bar{\rho}_e$ is larger than the mean value of the atmospheric density over a solar cycle, and rises otherwise;
- the shape of the proton energy spectra agrees rather well with experiment but the CRAND source is too weak to reproduce the observed intensities.

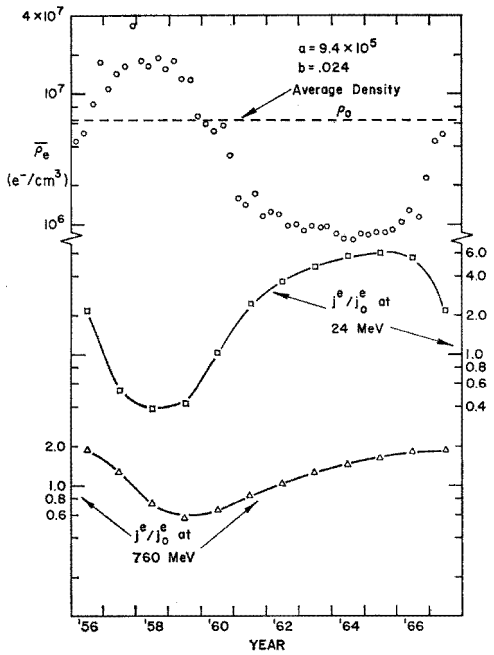

Fig. 2.2 The response of the unidirectional equatorial flux to the atmospheric variations over a solar cycle at $L_m = 1.6$ and $B_m = 0.23$ for 24 and 760 MeV protons. The fluxes j^e and j_0^e are computed by using a time dependent and a time independent atmosphere, respectively. From [2.12].

The CRAND problem is bypassed by presenting, instead of the flux itself, the ratio of the flux with a steady state solution. A typical result of the model is shown on Fig. 2.2 where flux ratios and the drift-shell averaged atmospheric density are compared at L_m = 1.6 and B_m = 0.23 for two different energies. The *B, L* values correspond to a drift shell with a minimum mirror point altitude of 510 km. At 24 MeV, the lifetime of the protons is short and the flux ratio almost inversely follows the atmospheric density. At 760 MeV, the flux ratio shows less variation due to the longer lifetime of the protons. The results depend on the values of *a* and *b*. For large values of *a*, the proton lifetime becomes shorter and the flux ratio inversely follows the atmosphere. For low values of *a*, the proton lifetime becomes greater and the hypotesises of the model are no more satisfied.

2.1.3 Macy et al. (1970) and Parsignault et al. (1981)

Macy et al. [2.23] and later on Parsignault et al. [2.24] presented a simple transport model to reproduce measurements of the 55-MeV proton fluxes over the time period from 1961 to 1976. For 1961 to 1971, the data are obtained from nuclear emulsions carried on recoverable polar US Air Force satellites. For 1972 to 1976, the data are obtained by solid state particle telescopes also aboard polar US Air Force satellites. Their model is designed for 55 MeV protons that reach low altitudes between 275 and 600 km. It includes:

- a time-independent source term that depends on energy and altitude, and the magnitude of which is fitted to reproduce the data at a given epoch;
- a friction term that represents the slowing down by atmospheric ionization function of time.

The energy dependence of both terms is represented by power laws. To be able to compare data and model, the transport equation has to be averaged over the South Atlantic Anomaly region at constant altitudes. Therefore, the friction term is set proportional to a mean atmospheric density that results from the averaging of drift-shell electronic atmospheric densities over B_m and L_m. The drift-shell densities are obtained with the modified Harris and Priester [2.18] atmosphere and the Hendricks and Cain geomagnetic field model [2.19] with the same procedure as Cornwall et al. [2.11]. Due to the simplicity of the model, the transport equation can be solved analytically for a finite period of time by assuming the atmospheric density as constant over that period. The time variation of the proton flux intensity is then evaluated with a 1-month time step by using the previous month's solution as input to the next month.

From the comparison between model and measurements at 275, 350 and 440 km altitudes, it results that:

- the Starfish explosion of July 1962 affects the 55-MeV proton population during 1-3 years, and, this Starfish additional population decays more rapidly at the lowest altitudes, where the atmospheric density is the highest;
- most of the time, there is a good agreement between model and experiment;
- the proton flux is underestimated by the model at solar maximum (1968-1970) and overestimated at very altitudes before the Starfish event.

The authors impute the discrepancies to the poor description of the source term which does not include a time variation nor an inward radial diffusion mechanism. Results at an altitudes of 350 km and 440 km are displayed in Fig. 2.3. In the left panel, the model is compared to the measurements at 350 km altitude during the sixties. The dashed vertical line corresponds to the time of the Starfish proton injection. The prediction for the "natural" protons is given by the solid curve while the result with the Starfish protons is given by the dashed curve. Both curves joins one year after the Starfish event. The starting point of the "natural" proton curve is overestimat-

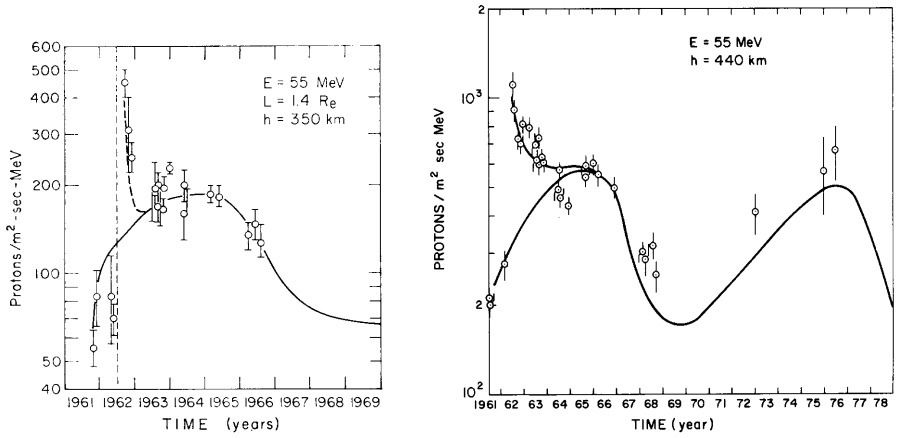

Fig. 2.3 Time variation of 55 MeV proton flux intensities at 350 and 440 km altitudes. The solid curves correspond to the model prediction with or without the Starfish injection of July 1962. The data points correspond to nuclear emulsion measurements. From [2.23] and [2.24].

ed in order to insure the model agreement with the 1964-1966 data. The right panel of Fig. 2.3 shows the flux variation over a whole solar cycle at an altitude of 440 km. At this higher altitude, it takes about 3 years to soften the effects of the Starfish explosion. During solar maximum, the model underestimated the proton flux intensity and an additional source mechanism is needed.

2.1.4 Bourdarie et al. (1997)

Bourdarie et al. [2.6] simulated the effects of a magnetic storm on radiation belt proton and electron population by solving a time-dependent Fokker-Planck equation in the 4-dimensional phase space (J_1, J_2, J_3, φ_3). The model called Salammbô is an extension of a previous three-dimensional model [2.5]. The azimuthal variable has been introduced in order to obtain a time resolution smaller than the drift particle period. The proton version of the model is designed for 1 keV to 300 MeV protons and includes:

- two friction terms due to the slowing down of protons by Coulomb scattering with plasmaspheric free electrons and with thermospheric bound electrons;
- a loss term due to charge exchange with atmospheric neutral hydrogen;
- a loss cone in equatorial pitch angle to emulate the open magnetic field line;
- an azimuthal transport term and a radial transport term both due to the particle drift which is caused by the magnetic field gradient, the corotation electric field and a time-dependent convective electric field.

Since the simulation covers only a time period of few days, neither internal source nor diffusion term were included. Note that a CRAND source and magnetic and electric radial diffusion terms are included in the three-dimensional model, but only steady state solutions of this model has been published [2.5]. A simple eccentric magnetic dipole is used to evaluate the different terms of the Fokker-Planck equation. For the simulation of the magnetic storm, the Salammbô model is initialized with distribution functions deduced from the NASA AP8 model, a short-time injection of low-energy protons at L = 9 in the night side, and a convection electric field that abruptly increases at the injection and then slowly recovers with a time constant of 800 s. The main results of the simulation:

- the very low energy protons are strongly influenced by the convection electric field and most of them are convected to the day side. Only a small part of the proton are transported inward, accelerated and trapped by the magnetic field;
- the model can well reproduce satellite measurements obtained by ATS 6 during a storm period. In particular, the drift echo is correctly reproduced;
- the ring current formation at $L = 4$ is clearly simulated.

The time evolution of the omnidirectional differential proton fluxes resulting from the simulation are presented in Fig. 2.4. The four panels show the flux profile on the night side as a function of the radial distance for four energies (5 keV, 50 keV, 100 keV and 1 MeV) and for different times: just before, just after, one hour after, and four hours after the injection (solid, dotted, dashed, and dot-dashed curves, respectively). The injection appears clearly at 5 and 50 keV. During the simulation, the peak of the flux intensity decreases and moves inward from $L = 9$ to the ring current region. Note that the inner part of the proton belt ($L < 3$) and high energy proton population ($E > 1$ MeV) are not affected by the injection and the recovery phase.

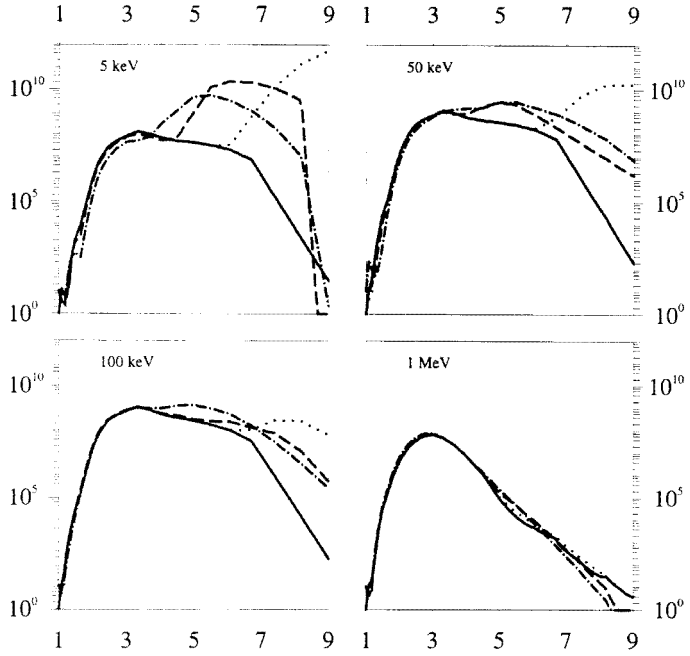

Fig. 2.4 Time evolution of proton omnidirectional differential fluxes (in $\mathrm{MeV}^{-1}\mathrm{cm}^{-2}\mathrm{s}^{-1}$) in the night side during a magnetic storm period as function of the radial distance (in Earth's radii). From [2.7].

2.1.5 Albert et al. (1998)

Albert et al. [2.1][2.2] applied a 2-dimensional Fokker-Planck equation to analyse the proton flux measurements of the PROTEL instrument aboard the CRRES satellite. The study concerns three time periods and is restricted to 1–100 MeV nearly equatorially mirroring protons with L values between 1.2 and 3. The time periods are from August 15, 1990 to March 18, 1991, from March 31 to May 31, 1991, and from June 23 to October 11, 1991. The periods are separated by the large magnetic storms of March 24 and June 4, 1991. The variation with L of the observed phase space density at $M = 200$ and 1000 MeV/G is shown on Fig. 2.5. The first period (squares and pluses) is assumed to be quiet but has a large depletion around $L = 2$ for $M > 200$ MeV/G. During both active periods (diamonds and crosses), the depleted region of the quiet period is

largely filled, and a second proton radiation belt clearly appears around $L = 2$. In the inner zone, at $L < 1.7$, the proton population is stable and is not affected by the magnetic storms. The Fokker-Planck equation defined in the (M,L) space is used to compute the steady state solution for each period, to compare the empirical values of the time variations of the phase space density function to time rates obtained from the diffusion equation, to apply a scenario to explain the L variation of the quiet period. It includes

- magnetic and electric radial diffusion terms, the coefficients of which are adapted for each period,
- a friction term due to the slowing down of protons by Coulomb scattering with plasmaspheric electrons,
- a loss term due to charge exchange with atmospheric neutral hydrogen,
- a CRAND source.

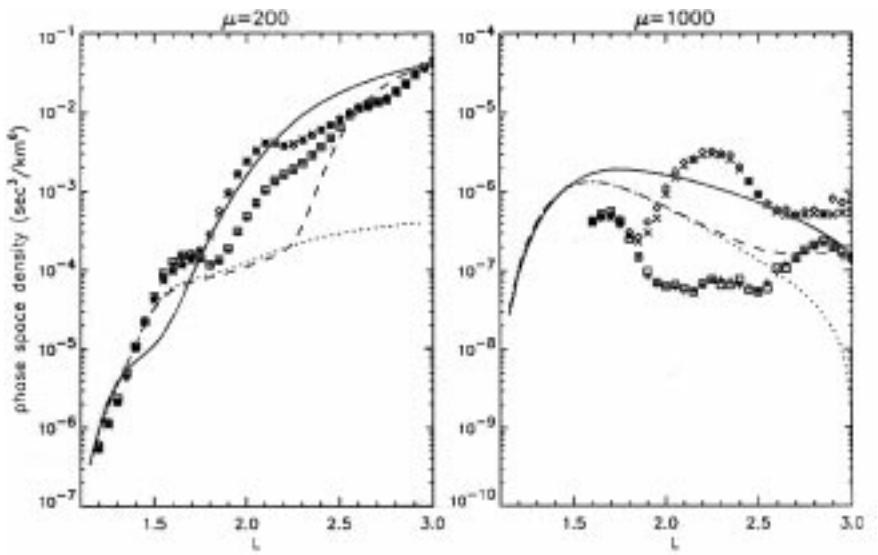

Fig. 2.5 The proton phase space density before (squares and pluses) and after (diamonds and crosses) the March 24 magnetic storm. The phase space density before the storm is compared to a steady state solution (solid curve) and a time varying diffusion simulation (dashed and dotted curves). From [2.1] and [2.2].

In the inner zone ($L < 1.7$), the steady state solutions of the Fokker-Planck equation (solid curve on Fig. 2.5) well reproduce the PROTEL data only up to $M = 200$ MeV/G. At higher energies, their disagreement with the measurements is attributed to a inaccurate description of the CRAND effect and/or to additional physical processes not present in the model. The main results of the time-dependent model are

- magnetic radial diffusion and Coulomb collisions dominate the time rates of change at most of the L and E values during the quiet period: the negative Coulomb term is gradually outweigh by a positive radial diffusion term with increasing L values;
- when the different terms of the Fokker-Planck equation nearly balance, the observed rates of change of the phase space density can not be reproduced;
- during active periods, the radial diffusion terms becomes negative at large L, and the observed rates of change differ from the quiet period mainly in the range $L = 2.2$–2.5;
- the depletion in the L profile of the quiet period can not be reproduced by a time-varying diffusion scenario where the boundary conditions are temporary reduced

The results of the time-varying scenario for the quiet period are shown by the dotted, dashed and solid curves on Fig. 2.5. The model is firstly initialized with the steady state solution fitted on the quiet model at $L = 3$ (solid lines). Then, during 1000 days, the outer boundary flux is decrease by a factor of 100, the Coulomb is increased by a factor of 5 and the radial diffusion is increased by a factor of 20. These changes are all made in order to reproduce the observed flux depletion (dotted lines). Afterward, the boundary conditions and different terms of the Fokker-Planck equation are restored to their initial values during 200 additional days. Unfortunately, the whole simulation (dashed line) shows that the boundary flux reduction does not diffuse sufficiently inward and that this time-varying diffusion scenario is not able to explain the observed flux profile. Albert et al. [2.2] speculate that the depletion was formed by a strongly nonadiabatic event.

2.2 Physical processes

Different models have been used to describe the dynamics of the proton radiation belt. Each model takes into account and neglects different physical processes. The processes can be classified by their location in Eq. (1.8): source, loss, friction and diffusive terms. In this section, we present the processes which can be relevant for the study of the inner edge of the proton radiation belt ($L < 2$).

2.2.1 Albedo neutron decay source

A flux of galactic cosmic rays reaches the Earth regularly. When entering the atmosphere, cosmic rays collide with nuclei (e.g. oxygen or nitrogen), produce neutrons, a part of which diffuses out into space. Due to their radioactive decay, these albedo neutrons contribute to inject protons inside the radiation belt. This cosmic ray albedo neutron decay (CRAND) remains the dominant source of high energy protons at low altitudes. Note that cosmic ray also produce albedo protons that could be trapped directly by the magnetic field. But, since after bouncing these protons will return approximately to their birth altitude or even lower, they will encounter a rather thick atmosphere and be rapidly lost. Albedo neutrons are also produced by solar protons when they collide with atmospheric components in the auroral regions. The solar proton albedo neutron decay (SPAND) corresponds to a source about ten times less intense as the CRAND source.

The theoretical computations and experimental measurements of the cosmic ray albedo neutrons has been extensively reviewed by White [2.30]. The neutron leakage flux j_n at the top of the atmosphere (i.e. about 50 km) depends on the neutron energy, the geomagnetic latitude λ at which a neutron leaves the Earth and the zenith angle ϕ made by the neutron velocity vector and the vertical. It is commonly accepted that these three dependencies can be treated separately. The j_n dependence on the geomagnetic latitude and the neutron energy spectrum are showed on Fig. 2.6 and Fig. 2.7, respectively. From both figures, one should note that

- less neutrons are produced in the equatorial region since the geomagnetic cut-off is higher at the equator than in the auroral region;
- the neutron energy spectrum highly differs from a simple spectral law, as found in early studies (e.g. by Singer [2.31] in 1958).

The dependence of j_n on the zenith angle is not well known. For high energy neutrons, an angular dependence of $\sec\phi$ seems the more appropriate[2.13][2.21]. Since neutron production depends on the cosmic ray flux, j_n varies during a solar cycle. It increases from solar maximum to solar minimum by about 25%[2.8].

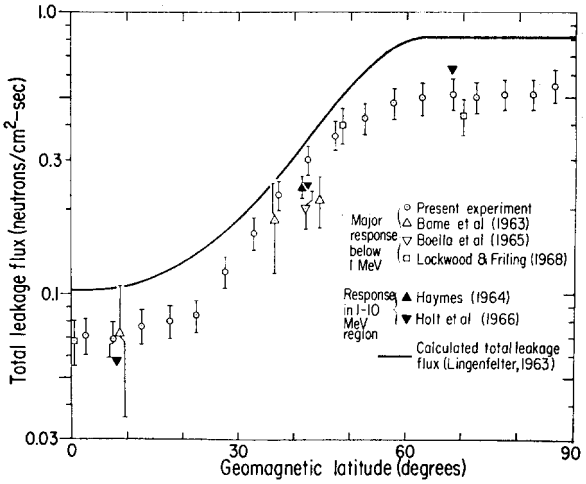

Fig. 2.6 Total neutron leakage flux as a function of the geomagnetic altitude, compilation of several neutron albedo flux measurements in the range 1–10 MeV. The solid curve results from a theoretical model. From [2.20].

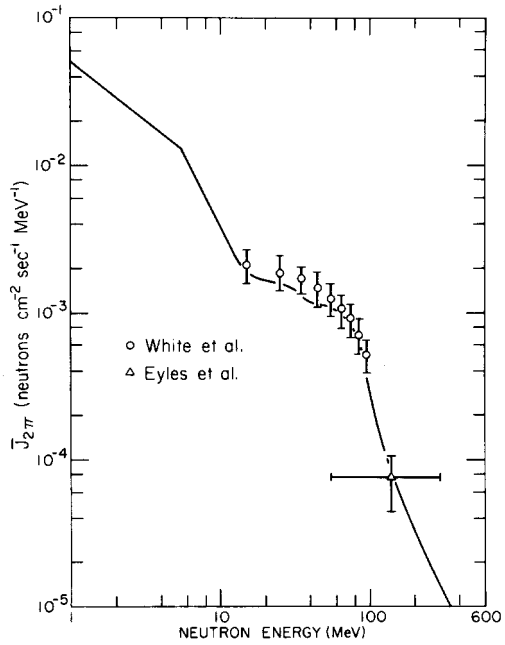

Fig. 2.7 Total neutron leakage flux as a function of the energy. The curve is based on measurements and Monte Carlo results. Specific observation at 50–100 MeV and 140 MeV are also displayed. From [2.10].

The solar proton albedo neutrons depends on the occurrence of solar flare. Compared to the cosmic ray albedo neutron, their energy spectrum is much steeper and their production is more concentrated at high latitude (see Fig. 5 and 9 in [2.22]).

The proton injection rate due to albedo neutron is usually evaluated for a drift shell under the assumptions that:

- the gravitation forces are negligible (the neutron gravitational potential at the Earth's surface is about 0.67 eV);

- the mean neutron lifetime $t_n = 1013\text{s}$ is long compared to its time of flight in the radiation belts;
- when decaying, the electron and antineutrino energies are negligible.

So, the neutrons are moving along a straight line, they decay anywhere along their trajectory with equal probability, and the direction of flight and the energy are fully transmitted from the neutron to the proton during the radioactive decay. At a given point along the drift shell, the proton injection is obtained by only taking into account the neutron with a correct local pitch angle α. The local injection rate is then given by

$$q(E, L, \alpha_0) = \frac{cm_0}{t_n\sqrt{E^2 + 2Em_0c^2}} \oint \frac{d\beta}{2\pi} j_n(E, \lambda, \phi) \tag{2.2}$$

where β is an azimuthal angle that covers all the directions of the α cone. In Eq. (2.2) the magnetic latitude and the zenith angle are function of both the pitch angle, the azimuthal angle and the starting positions[2.21]. When the direction (α, β) does not intersect the Earth's surface, j_n is zero. The local injection rate has to be averaged over the whole drift shell.

2.2.2 Atmospheric absorption

Protons can be absorbed during their travel trough the atmosphere by charge exchanges and inelastic nuclear interactions. It is generally admitted that charge exchange represents an important mechanism for removal at energies lower than 1 MeV and nuclear interaction losses at energies higher than 500 MeV. For both mechanisms, the absorption rate is given by

$$\Lambda = v\sum_i \rho_i \sigma_i \tag{2.3}$$

where the sum runs over the different atmospheric components, ρ_i is the density of component i, σ_i is the cross section for inelastic nuclear collisions and charge exchange, and v is the proton velocity.

Fig. 2.8 Charge exchange cross section for proton in hydrogen, helium, oxygen and nitrogen gases. Based on [2.3].

The charge exchange reaction transforms a trapped proton into neutral hydrogen by the transfer of an electron from an atmospheric ion, atom or molecule. Such a reaction only occurs at low altitudes and for low energy protons. Cross sections for some atmospheric constituents as a

function of the incident proton energy are shown on Fig. 2.8. The figure is based on the compilation of Allison [2.3]. Note that, except for Helium, the given cross sections correspond to charge exchanges in molecular gas. It appear clearly that a charge exchange only occurs for protons of energy less than 1 MeV.

Energetic protons can experiment inelastic nuclear collisions with atmospheric constituents such as nitrogen or oxygen. During these inelastic nuclear collisions, the proton can be absorbed or slow down and deviated, secondary protons can be produced as well as other particles such as neutrons, light nuclei, etc. It is generally assumed that the incident proton does not remain geomagnetically trapped after the inelastic nuclear collisions and that no secondary protons are produced. In that case, Eq. (2.3) can be used the oxygen and nitrogen total reaction cross sections. For $p + {}^{16}O$ inelastic nuclear collisions, the total cross section can be approximately fitted as

$$\begin{aligned} \sigma &= 274 + 191 \log_{10} E \text{ when } E < 24 \text{ MeV} \\ \sigma &= 1127 - 427 \log_{10} E \text{ when } 24 < E < 95 \text{ MeV} \\ \sigma &= 282 \text{ when } E > 95 \text{ MeV} \end{aligned} \tag{2.4}$$

where the energy and the cross section are expressed in MeV and mb, respectively. The fit is based on experimental data ranging from 20 to 570 MeV [2.9][2.26]. Due to the lack of data for the $p + {}^{14}N$ reaction [2.4], the total cross section can be obtained by multiplying the cross section of Eq. (2.4) by the factor $(14/16)^{2/3}$.

2.2.3 Trapping breakdown

Protons can be diffused or transported into an unstable trapping region, i.e. a region where M, J or Φ are not more defined or invariant. Different situations can cause a breakdown of the adiabatic conditions.

Open field line at high latitudes

Above the auroral region, the magnetic field lines extend indefinitely to the geomagnetic tail. They are linked to the interplanetary magnetic field or they are close through the neutral sheet In this region, charged particles bounce eventually once time and then escape from the vinicity of the Earth: they are not trapped any more. Note that the first adiabatic invariant can still be defined.

Quasi-trapped particles

In some parts of the outer magnetosphere, the guiding centre of charged particles can be located on a close magnetic field line, such that both first adiabatic invariant are well defined, but the particles are unable to complete a whole drift around the Earth [2.27]. The particles are quasi-trapped. In particular, particles mirroring at low latitudes on the night side at L about 8 abandon the Earth's magnetosphere before reaching the noon meridian, and, particles mirroring at high latitudes on the day side run into the tail before reaching the midnight meridian. The location of the quasi trapping regions is illustrated on Fig. 2.9.

Breakdown at high energies

At high energies, when the Larmor radius of the particle is too large with respect of the magnetic field curvature, the invariance of M or J can be breakdown. The particle orbits become then un-

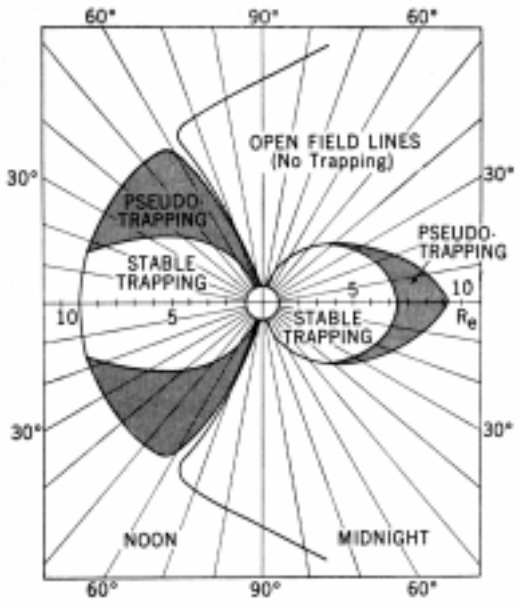

Fig. 2.9 Location of the quasi-trapping regions in the equatorial plane. From [2.27]

stable and the particles can be lost from the trapped region. The breakdown of the adiabatic conditions based on the Alfvén discriminant gives a cutoff energy varying as L^{-4} [2.29]. The dependence of the cutoff energy in L has been also studied by numerical simulation [2.15].

2.2.4 Atmospheric ionization and excitation

In the atmosphere, the protons lose energy by ionization and excitation of the nitrogen and oxygen atoms at low altitudes, of helium and hydrogen at higher altitudes. The theory of the energy loss of fast charged particles by ionisation and excitation was first established by Bohr through a semi-classical procedure. A quantum-mechanical formulation was proposed later by Bethe. The average energy loss per unit pathlength is related to the cross section for all possible individual collision by

$$-\frac{dE}{dx} = \sum_i \rho_i \sum_n \Delta E_n \sigma_{ni} \tag{2.5}$$

where σ_{ni} is the cross section for the inelastic collision which raises an atom of type i to an energy level ΔE_n above its ground state. The stopping power theory leads to the formula [2.14]

$$-\frac{dE_i}{dx} = \frac{4\pi q^4}{m_e v^2}\rho_i Z_i\left(\ln\frac{2m_e v^2}{I_i} - \ln\left[1-\frac{v^2}{c^2}\right] - \frac{v^2}{c^2} - \frac{C_i}{Z_i}\right) \tag{2.6}$$

where m_e is the electron rest mass, q is the electronic charge, Z_i, I_i and C_i are the atomic number, the average excitation and ionization potential and the inner shell correction of the absorber i, respectively. The factor in the braces of Eq. (2.6) is a slowly monotonously increasing function of the proton energy. It predominates only at very low energies and at extremely high energies. In the intermediate energy range, i.e. 1 MeV–1 GeV, the first factor dominates and causes the stopping power to decrease with increasing proton energy. Estimated values of I_i are

Table 2.1 Average excitation and ionization potential. From [2.14]

Substance	Z	I	Reference
Molecular hydrogen	1	18.3	Martin, F.W., and Northcliffe, L.C., 1962: Phys. Rev. 128, 1166
Helium	2	42.0	Brolley, J.R., and Ribe, F.L., 1955: Phys. Rev. 98, 1112
Molecular nitrogen	7	88.0	Thompson, T.J., 1952: Univ. Calif. Radiation Lab. Rept. No. 1910
Molecular oxygen	8	101.0	Thompson, T.J., 1952: Univ. Calif. Radiation Lab. Rept. No. 1910

given in Table 2.1. The inner shell correction plays a role mainly at large atomic numbers and low proton energies [2.14].

2.2.5 Multiple angular scattering

Multiple Coulomb scattering causes diffusion in particle pitch angle. For protons, this effect is small and generally neglected. Nevertheless, at very low altitudes, a slight change in pitch angle can produce a rather large change in the location of the mirror points and in the average atmospheric density experienced by the proton [2.12]. The mean square deflection can be obtained from the differential cross section $\sigma(E, \theta)$ by

$$\Delta\alpha^2 = 2\pi\int_0^{\pi} \theta^2 \sigma(E, \theta) \sin\theta d\theta \tag{2.7}$$

Using a screened Coulomb potential, the elastic scattering cross section can be written as

$$\sigma(E, \sigma) = \frac{Z^2 e^4}{m_R^2 v^4} \frac{1}{(1 + 2\eta - \cos\Theta)^2} \tag{2.8}$$

where m_R is the reduced mass and η the phase shift. The phase shift can be approximated evaluated by

$$\eta = \frac{1}{2}\left(\frac{Z^{1/3} h}{5.561 m_R v a_0}\right) \tag{2.9}$$

where h is the Planck constant and a_0 the radius of the first Bohr orbit [2.25].

2.2.6 External field fluctuations

Drift-resonant fluctuations in the magnetospheric magnetic field and in the convection electric field induce a violation of the third invariant and a radial diffusion of the trapped particles. A formal expression for the radial diffusion coefficients has been obtain by theoretical analysises and is typically given by [2.28]

$$D_{LL} = A_m L^{10}\left(\frac{Q(\sin\alpha_0)}{180 D(\sin\alpha_0)}\right)^2 + A_e L^{10} \frac{\gamma^2 \sin^4\alpha_0 / M^2}{1 + (\Omega\tau)^{-2}} \left(\frac{T(\sin\alpha_0)}{2D(\sin\alpha_0)}\right)^2 \tag{2.10}$$

where L is the Roederer's shell parameter [see Eq. (1.10)], γ is the relativistic factor, $A_m = 8.1\ 10^{-14}\mathrm{s}^{-1}$, $A_e = 1.16\ 10^{-15}\mathrm{s}^{-1}\mathrm{G}^{2}\mathrm{GeV}^{-2}$ τ is the mean e-folding time of an electrostatic impulse and is about 1200s,

$$\Omega = \frac{3cLR_E}{M_0}\ \frac{p^2}{m}\ \frac{D(\sin\alpha_0)}{T(\sin\alpha_0)} \tag{2.11}$$

is the drift frequency, and T, D and Q are functions well approximated in a dipolar field by

$$T(y) \approx 1.380173 - 0.639693y^{3/4} \tag{2.12}$$

$$D(y) \approx \frac{1}{12}(5.520692 - 2.35194y + 1.279385y^{3/4}) \tag{2.13}$$

$$Q(y) \approx -27.12667 - 45.39913y^4 - 5.88256y^8 \tag{2.14}$$

One should note that due to its dependence in L, the radial diffusion coefficients of Eq. (2.10) do not play an important role in the inner edge of the radiation belt.

References

[2.1] Albert, J.M., G.P. Ginet and M.S. Gussenhoven, 1998: CRRES observations of radiation belt protons 1. Data overview and steady state radial diffusion, J. Geophys. Res., to be published

[2.2] Albert, J.M., and G.P. Ginet, 1998: CRRES observations of radiation belt protons 2, Time-Dependent Radial Diffusion, J. Geophys. Res., to be published

[2.3] Allison, S.K., 1958: Experimental results on charge-changing collisions of hydrogen and helium atoms and ions at kinetic energies above 0.2 keV, Rev. Mod. Phys. 30, 1137–1168

[2.4] Bauhoff, W., 1986: Tables of reaction and total cross sections for proton-nucleus scattering below 1 GeV, Atomic Data and Nuclear Data Tables 35, 429–447

[2.5] Beutier, T., D. Boscher and M. France, 1995: SALAMMBO: A three-dimensional simulation of the proton radiation belt, J. Geophys. Res. 100, 17181-17188

[2.6] Bourdarie, S., D. Boscher, T. Beutier, J.-A. Sauvaud and M. Blanc, 1997: Electron and proton radiation belt dynamic simulations during storm periods: A new asymmetric convection-diffusion model, J. Geophys. Res. 102, 17541-17552

[2.7] Bourdarie, S., 1996: Modélisation de la dynamique des ceintures de radiations à l'échelle de l'orage magnétique, PhD thesis, n° 198, ENSAE, Toulouse, France

[2.8] Blanchard, R.C., and W.N. Hess, 1964: Solar Cycle Changes in Inner-Zone Protons, J. Geophys. Res. 69, 3927-3938

[2.9] Carlson, R.F., A.J. Cox, J.R. Nimmo, N.E. Davison, S.A. Elbakr, J.L. Horton, A. Houdayer, A.M. Sourkes, W.T.H. van Oers and D.J. Margaziotis, 1975: Proton total reaction cross sections for the doubly magic nuclei 16O, 40Ca, and 208Pb in the energy range 20-50 MeV, Phys Rev C 12, 1167–1175

[2.10] Claflin, E.S., and R.S. White, 1974: A study of equatorial inner belt protons from 2 to 200 MeV, J. Geophys. Res. 79, 959-965

[2.11] Cornwall, J.M., A.R. Sims and R.S. White, 1965: Atmospheric Density Experienced by Radiation Belt Protons, J. Geophys. Res. 70, 3099-3111

[2.12] Dragt, A.J., 1971: Solar Cycle Modulation of the Radiation Belt Proton Flux, J. Geophys. Res. 76, 2313-2344

[2.13] Dragt, A.J., M.M. Austin and R.S. White, 1966: Cosmic Ray and Solar Proton Albedo Neutron Decay Injection, J. Geophys. Res. 71, 1293-1304

[2.14] Fano, U., 1963: Penetration of prtons, alpha particles and mesons,Ann. Rev. Nucl. Sci. 13, 1–66

[2.15] Garmire, G., 1963: Geomagnetically Trapped protons with energies greater than 350 MeV, J. Geophys. Res. 68, 2627–2638

[2.16] Harris, I., and W. Priester, 1962: Theoretical Models for the Solar-Cycle Variation of the Upper Atmosphere, J. Geophys. Res. 67, 4585-4591

[2.17] Harris, I., and W. Priester, 1962: Time-Dependent Structure of the Upper Atmosphere, J. Atmospheric Sci. 19, 286

[2.18] Harris, I., and W. Priester, 1963: Relation between theoretical and observational models of the upper atmosphere, J. Geophys. Res. 68, 5891-5894

[2.19] Hendricks, S.J., and J.C. Cain, 1966: Magnetic Field Data for Trapped-Particle Evaluations, J. Geophys. Res. 71, 346-347

[2.20] Jenkins, R.W., J.A. Lockwood, S.O. Ifedili and E.L. Chupp, 1970: Latitude and altitude dependence of the cosmic ray albedo neutron flux, J. Geophys. Res. 75, 4197-4204

[2.21] Lenchek, A.M., 1962: On the anomalous component of low-energy geomagnetically trapped protons, J. Geophys. Res. 67, 2145-2157

[2.22] Lingenfelter, R.E., and E.J. Flamm, 1964: Neutron leakage flux from interactions of solar protons in the atmosphere, J. Geophys. Res. 69, 2199-2207

[2.23] Macy, W.W., R.S. White, R.C. Filz and E. Holeman, 1970: Time variations of radiation belt protons, J. Geophys. Res. 75, 4322-4328

[2.24] Parsignault, D.R., E. Holeman and R.C. Filz, 1981: Solar Cycle Induced Modulation of the 55-MeV Proton Fluxes at Low Altitudes, J. Geophys. Res. 86, 11439-11442

[2.25] Rees, M.H., 19??: Physics and chemistry of the upper atmosphere, Cambridge university press, Cambridge.

[2.26] Renberg, P.U., D.F. Measday, M. Pepin, P. Schwaller, B. Favier and C. Richard-Serre, 1972: Reaction cross sections for protons in the energy range 220-570 MeV, Nucl. Phys. A183, 81–104

[2.27] Roederer, J.G., 1967: On the adiabatic motion of energetic particles in a model magnetosphere, J. Geophys. Res. 74, 981–992

[2.28] Schulz, M., 1991: The Magnetosphere, in Geomagnetism, vol. 4, ed. P. Jacobs, Academic Press, 87-293

[2.29] Singer, S.F., 1959: On the cause of the minimum in the earth's radiation belt, Phys. Rev. Letters 3, 188–

[2.30] White, R.S., 1973: High-energy proton radiation belt, Rev. Geophys Space Phys. 11, 595-632

[2.31] Singer, S.F., 1958: Radiation belt and trapped cosmic ray albedo, Phys. Rev. Lett. 1, 181-